28. Shepherd, G. M. G., Assad, J. A., Prarakkal, M., Kachar, B. & Corey, D. P. Movement of the tip-link attachment is correlated with adaptation in bullfrog saccular hair cells. *J. Gen. Physiol.* **98,** 25A (1991).
29. Nagafuchi, A. & Takeichi, M. Cell binding function of E-cadherin is regulated by the cytoplasmic domain. *EMBO J.* **7,** 3679–3684 (1988).

Supplementary Information accompanies the paper on **www.nature.com/nature**.

Acknowledgements We thank R. Kemler for E-cadherin clones; M. Senften for L929 cells expressing E-cadherin; T. Hasson, B. Ranscht and H. C. VanSteenhouse for technical advice; and A. Kralli, L. Stowers and A. Patapoutian for critical reading of the manuscript. J.S. was supported by a fellowship from the Boehringer Ingelheim Fonds; A.R. by a C. J. Martin Fellowship from the National Health and Medical Research Council (Australia). This work was supported by grants from the NIDCD and NEI (U.M, P.G.G. and D.S.W.).

Competing interests statement The authors declare that they have no competing financial interests.

Correspondence and requests for materials should be addressed to U.M. (umueller@scripps.edu).

Mutations in *cadherin 23* affect tip links in zebrafish sensory hair cells

Christian Söllner[1], Gerd-Jörg Rauch[2], Jan Siemens[4], Robert Geisler[2], Stephan C. Schuster[3], the Tübingen 2000 Screen Consortium*, Ulrich Müller[4] & Teresa Nicolson[1,5]

[1]*Max-Planck-Institut für Entwicklungsbiologie, Spemannstrasse 35, 72076 Tübingen, Germany*
[2]*Abteilung Genetik,* [3]*AG Genomics & Signal transduction, Max-Planck-Institut für Entwicklungsbiologie, Spemannstrasse 35, 72076 Tübingen, Germany*
[4]*The Scripps Research Institute, 10550 N. Torrey Pines Road, Mail Drop ICND222, La Jolla, California 92037, USA*
[5]*Oregon Hearing Research Center and Vollum Institute, 3181 SW Sam Jackson Park Road, Portland, Oregon 97239, USA*

* A list of members of the Tübingen 2000 Screen Consortium and their affiliations appears at the end of the paper

Hair cells have highly organized bundles of apical projections, or stereocilia, that are deflected by sound and movement. Displacement of stereocilia stretches linkages at the tips of stereocilia that are thought to gate mechanosensory channels[1]. To identify the molecular machinery that mediates mechanotransduction in hair cells, zebrafish mutants were identified with defects in balance and hearing[2]. In *sputnik* mutants, stereociliary bundles are splayed to various degrees, with individuals displaying reduced or absent mechanotransduction[3,4]. Here we show that the defects in *sputnik* mutants are caused by mutations in *cadherin 23* (*cdh23*). Mutations in *Cdh23* also cause deafness and vestibular defects in mice and humans[5–9], and the protein is present in hair bundles[10,11]. We show that zebrafish Cdh23 protein is concentrated near the tips of hair bundles, and that tip links are absent in homozygous *sputnik*^{tc317e} larvae. Moreover, tip links are absent in larvae carrying weak alleles of *cdh23* that affect mechanotransduction but not hair bundle integrity. We conclude that Cdh23 is an essential tip link component required for hair-cell mechanotransduction.

Stereocilia are interconnected by extracellular filaments, and several linkages have been identified on the basis of their position along the bundle and sensitivity to proteases or calcium chelators[12–17]. These include ankle links near the base of the bundle, lateral links or shaft connectors in the medial part, and tip links near the stereociliary tips. Tip links are postulated to be a part of the mechanotransduction apparatus and are thought to physically tug open transducer channels when bundles are deflected in the excitatory direction[18]. The other links appear to make important structural contributions to bundle architecture and stiffness. Although some biochemical properties have been characterized[12–16], the molecular identity of these extracellular filaments is unknown. One exception is the lower lateral links, also called shaft connectors, which are absent in protein tyrosine phosphatase receptor Q knockout mice[17]. In addition, mutations that disrupt the integrity of hair-cell bundles in animal model organisms have identified unconventional myosins and novel cadherins as having a function in normal bundle formation and integrity[19,20].

In zebrafish, several auditory and vestibular mutants have been described with defects in bundle integrity[3,20]. Mutant *sputnik* larvae have splayed hair bundles and mechanotransduction is affected[3,4]. The recessive alleles of *sputnik* vary in strength, ranging from an obvious defect in bundle integrity and lack of extracellular receptor potentials to a fairly weak phenotype in which very few bundles are splayed and yet extracellular potentials are reduced by two-thirds.

To identify *sputnik*, we meiotically mapped the *sputnik* locus (allele *tj264a*), defining the critical interval by scoring over 2,500 homozygous mutant larvae with polymorphic markers (Fig. 1a). A chromosomal walk was initiated and a clone within the critical interval, PACc (BUSMP706A1551Q0), was shotgun sequenced (Fig. 1a). Four exons of *cdh23* were found on PACc and rapid amplification of cloned ends with polymerase chain reaction (RACE PCR) was used to generate the full-length sequence. Zebrafish *cdh23* encodes a 3,366 amino acid protein containing 27 ectodomains or extracellular repeats followed by a single transmembrane domain and a carboxy-terminal tail (Fig. 1b). The zebrafish Cdh23 protein is 68% identical and shares 81% similarity with the respective human and mouse CDH23 proteins[5–9]. Using PCR with reverse transcription (RT), we detected two additional splice variants of *cdh23* messenger RNA (Fig. 1b). Exon 68, which encodes a portion of the intracellular domain, is present only in the full-length form. We sequenced complementary DNAs from homozygous mutant larvae and detected nonsense and missense mutations, or insertions (Fig. 1b).

To determine where *cdh23* was expressed, we examined mRNA levels using *in situ* hybridization. mRNA was first detected in the embryonic ear at 24 h post-fertilization (h.p.f.) and at all later stages (Fig. 1c–e). The two patches of cells, which are clearly labelled at opposite ends of the otic vesicle, are the first hair cells to develop and express hair-cell-specific genes[20,21] (Fig. 1c). At later stages, *cdh23* mRNA was also detected in the brain, olfactory organ and in a subset of cells within the eye (data not shown). In the neuroepithelium of the ear and lateral line neuromasts, *cdh23* was expressed exclusively in hair cells (Fig. 1d, e). Hybridization with a sense probe did not yield a detectable signal (Supplementary Fig. 1).

In live, undissected *sputnik* larvae, detachment of bundles from kinocilia or splaying of stereocilia is visible, albeit at low resolution[3]. In order to assess the differences between the various alleles in *sputnik* larvae in more detail, we examined fluorescently labelled bundles in intact fixed larvae (Fig. 2). In larvae carrying a frameshift resulting in a nonsense mutation (*tc317e*), almost all (94%) of the bundles showed some splaying or were disorganized (Fig. 2b, i; $n = 48$ bundles). A similar percentage of bundles was also affected in *sputnik*^{t23576} larvae carrying a nonsense mutation (data not shown). Many bundles were splayed in *sputnik*^{tj264a} (74%) and *sputnik*^{tc242b} (59%) larvae, but intact bundles were also present (Fig. 2c, d, i; $n = 54$ and $n = 44$ bundles, respectively). It is worth noting that hair bundles treated with BAPTA exhibit severe splaying and have a broad, fan-like appearance[15], suggesting that the stronger alleles of *cdh23* do not cause complete splaying. Indeed, transmission electron microscopy (TEM) analysis suggests that the degree of splaying of stereocilia in *sputnik*^{tc317e} mutants is not severe (see Supplementary Fig. 2). In the weaker allele, *tz300a*, splaying was present (38%); however, over half of the bundles appeared to be unaffected and the degree of splaying was more subtle (Fig. 2e, i; $n = 39$ bundles). Finally, in larvae carrying the

weakest allele, *te370e*, only 5% of the bundles were splayed whereas the others appeared to be unaffected (Fig. 2f, i; $n = 52$ bundles).

We sought to mimic a null situation by inhibiting translation or splicing of *cdh23* mRNA (Fig. 2k). Antisense morpholino-modified oligonucleotides (morpholinos) against *cdh23* mRNA were injected into wild-type embryos at the one- to two-cell stage. At 5 days post-fertilization (5 d.p.f.), we observed pronounced vestibular or balance defects that were dose-dependent (Fig. 2j). In contrast, injection of mismatched morpholinos at the highest concentration (45 ng) did not cause circling behaviour (Fig. 2j). Splaying of bundles in morpholino-injected larvae (morphants) was comparable to the splaying seen in the strongest alleles of *sputnik* (Fig. 2 g, h). No other obvious defects were detected in morpholino-injected larvae.

Our data indicate that strong alleles of the zebrafish *cdh23* gene that are expected to inactivate its function cause splaying of stereocilia and defects in balance and hearing. This resembles the phenotype of *Cdh23*-deficient mice, which also have disorganized stereocilia[7]. Notably, weaker alleles of *cdh23* cause less severe defects in zebrafish hair bundles, yet still lead to circling behaviour and reduced extracellular receptor potentials. These findings suggest that Cdh23 not only functions in maintaining bundle integrity, but may also have a direct role in mechanotransduction.

Using confocal microscopy, we immunolocalized Cdh23. We labelled intact zebrafish larvae with an antibody directed against the cytoplasmic domain of murine CDH23 (amino acids 3,133–3,291). This antibody cross-reacts with Cdh23 from many different species[22]. Immunoreactivity was present at the distal tips of hair bundles, especially the tallest stereocilia next to the kinocilia (Fig. 3a). In teleost fish, kinocilial links between the kinocilia and adjacent stereocilia are highly concentrated in this region[23]. Higher magnification views showed labelling of shorter stereocilia as well

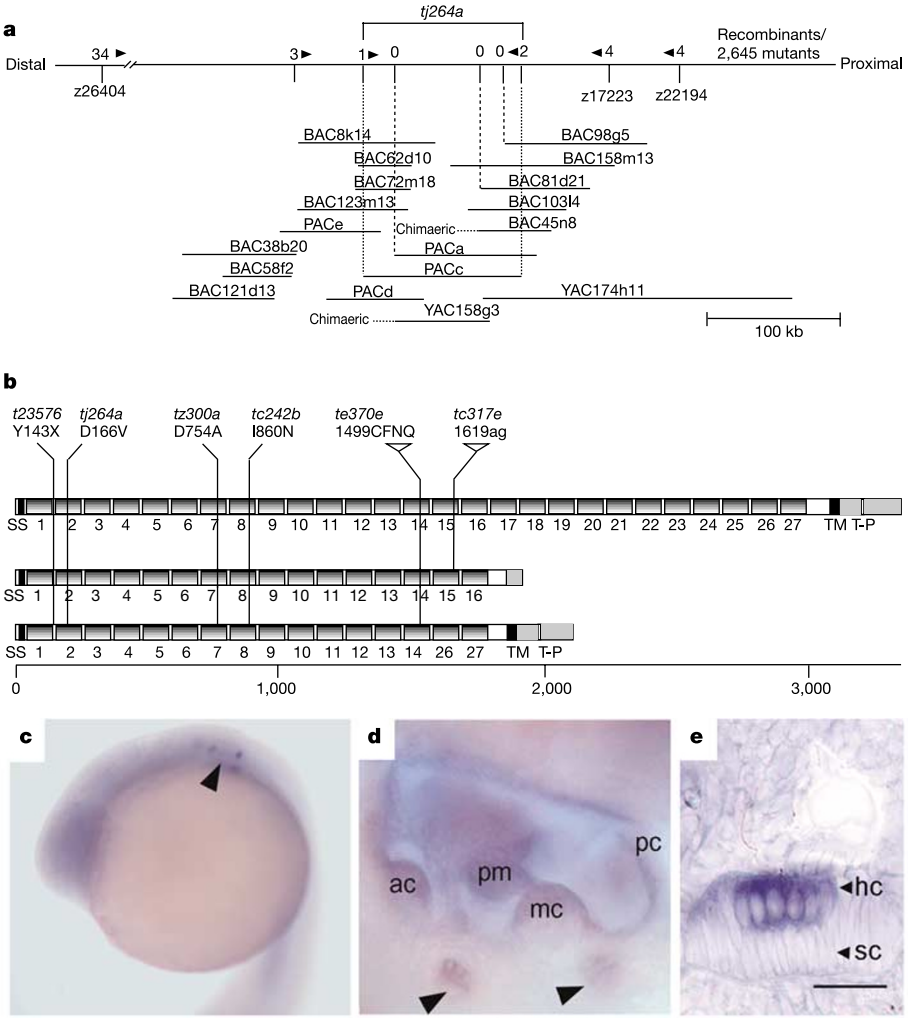

Figure 1 Positional cloning of *sputnik* and identification of the mutations in *cdh23*. **a**, Integrated genetic and physical map of the region on LG13 containing the *tj264a* mutation. The PACc clone (115 kb) contained four exons encoding 704 bp of the *cdh23* gene and no other open reading frames. **b**, The zebrafish *cdh23* gene encodes a 3,366-amino-acid protein containing a signal sequence (SS), 27 ectodomains, a single-pass transmembrane domain (TM) and a tyrosine phosphorylation site (T-P). All the mutations are located in ectodomains. *tj264a*, *tz300a* and *tc242b* are missense mutations. In *te370e* there is an insertion of four amino acids in EC14. The *tc117e* mutation consists of the insertion of two nucleotides causing a frameshift, leading to a premature stop codon at amino acid position 1,629. The *tc23576* allele contains a transversion leading to a stop codon at amino acid position 143 located between EC1 and EC2. **c**, **d**, Expression of *cdh23* mRNA at various stages of development in zebrafish larvae. Whole-mount *in situ* hybridization of *cdh23* in a 24 h.p.f. embryo (**c**) and a 5 d.p.f. larva (**d**, **e**). **c**, Lateral view of *cdh23* mRNA expression in the sensory cells of the otic placode (arrowhead). **d**, Ear of a larva at 5 d.p.f. with staining of the neurosensory epithelium. In addition, two neuromasts at the surface (arrowheads) are visible. ac, anterior crista; mc, medial crista; pc, posterior crista; pm, posterior macula. **e**, Thick section of an anterior macula. hc, hair cell; sc, supporting cell. Scale bar in **e** indicates 50 μm in **c**, **d** and 10 μm in **e**.

(Fig. 3c, arrows). This pattern is very similar to the Cdh23 staining pattern in bullfrog and mouse hair cells (see the accompanying manuscript[22]), and to the staining described in chick hair cells labelled with antibodies against a tip link antigen[16]. In contrast to wild-type bundles, stereocilia in *sputnik*^{t23567} mutants, which carry a nonsense allele causing a truncation after ectodomain 1 (EC1), did not show immunoreactivity, confirming the specificity of staining at bundle tips (Fig. 3b). In addition, immunoreactivity present in the retina in wild-type larvae was absent in *sputnik*^{t23567} mutants (data not shown).

The size and predicted topology of Cdh23 along with the localization pattern raised the possibility that Cdh23 may constitute one of the extracellular links or filaments that connect individual stereocilia. Previous studies have shown that both rigidification and *cis* and *trans* interactions between cadherins require calcium[24]. Moreover, both the ankle link and tip link are sensitive to calcium chelators[15,25], and hair bundles exhibit severe splaying after prolonged exposure to BAPTA[15]. We therefore examined the integrity of extracellular links in larvae carrying the frameshift mutation in *cdh23* (*tc317e*) by electron microscopy. Because the frameshift leads to a truncation within EC15, this mutation is predicted to cause a null phenotype. Although confocal images of *sputnik*^{tc317e} hair bundles suggest that the degree of splaying is pronounced, at the electron microscopic level many stereocilia are still associated with each other in bundles (Supplementary Fig. 2). Hence, despite the presence of splaying in *sputnik*^{tc317e} hair bundles, we expected to be able to visualize the linkages between adjacent stereocilia. We examined over 200 serial sections of 19 individual hair bundles in the anterior macula of five different *sputnik*^{tc317e} larvae at the electron microscopic level and did not observe any tip links (Fig. 3g, i), which extend obliquely from stereociliary tip densities to insertion plaques on adjacent stereocilia as seen in wild-type siblings (Fig. 3h). Insertion plaques were also absent. Although the stereociliary tips in mutants often appeared slightly darker or electron dense, the asymmetrical shape or tenting of stereocilia that was

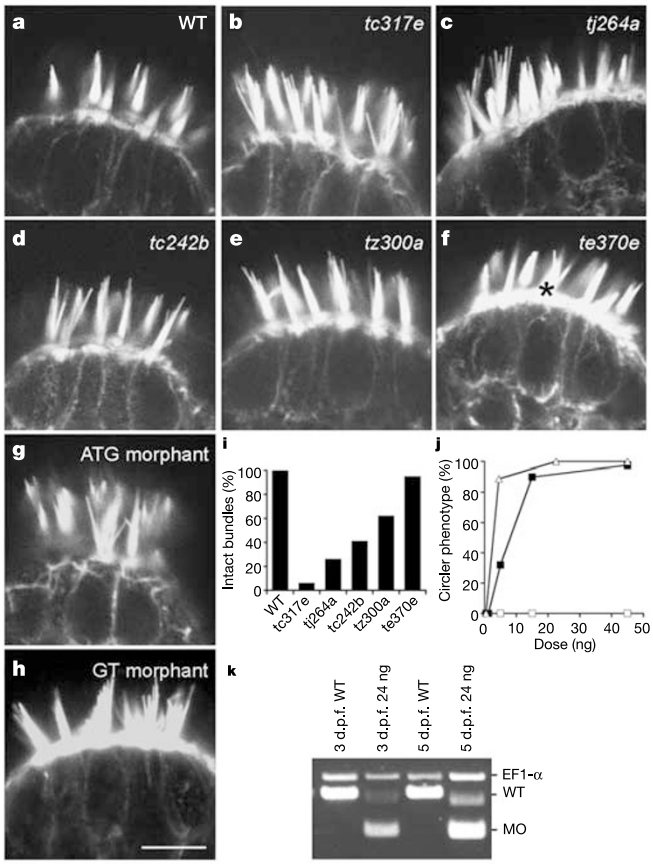

Figure 2 Confocal images of splaying of inner ear hair bundles in mutant *sputnik* larvae and *cdh23* morphants (5 d.p.f.). **a**, Medial ampullary hair bundles stained with Alexa-fluor-488–phalloidin in a wild-type larva. **b**–**d**, Hair bundles in larvae carrying the *tc317e* (**b**), *tj264a* (**c**) and *tc242b* (**d**) alleles show obvious defects in bundle integrity. **e**, A weaker allele, *sputnik*^{tz300a}, shows more subtle degrees of splaying. **f**, Most of the bundles in *sputnik*^{te370e} larvae are intact. A splayed bundle is indicated by an asterisk. **g**, **h**, Examples of bundle splaying in morphants injected with *cdh23* antisense morpholinos (45 ng). ATG morpholinos block initiation of mRNA translation, whereas GT morpholinos interfere with mRNA splicing events (see panel **k**). Scale bar: 5 μm. **i**, Graphic presentation of the intact percentage of hair bundles in each allele. **j**, Dose–response curve for ATG (filled squares), GT (open triangles) and mismatched *cdh23* morpholinos (open squares). Each dose point indicates the percentage of larvae at 5 d.p.f. ($n \geq 30$) with balance defects and summarizes the results from three separate injection experiments. **k**, RT–PCR products of full-length (middle band) and aberrantly spliced *cdh23* message (lower band missing the second coding exon of 78 bp) from pools of uninjected (WT) and injected (24 ng GT morpholino) animals. As a control, we included *elongation factor 1 alpha* (EF1-α) primers (upper band).

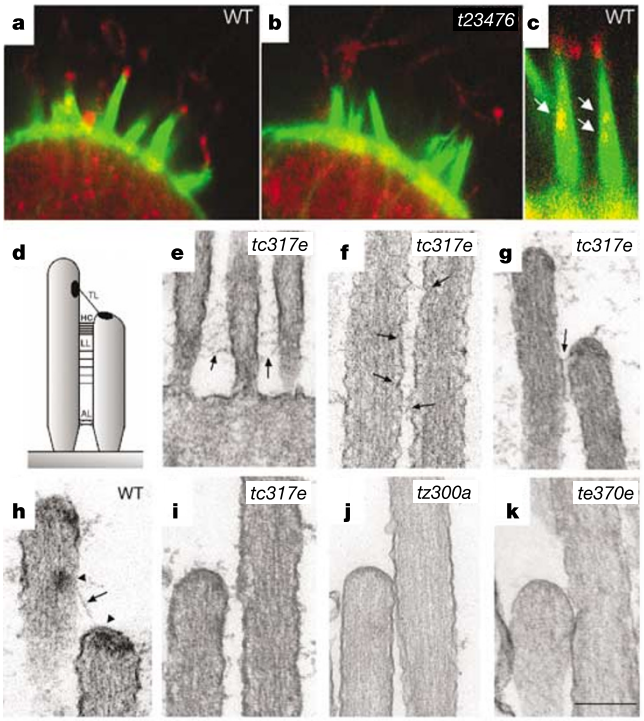

Figure 3 Localization of Cdh23 to hair bundles and absence of tip links in *sputnik* mutants. **a**–**c**, All confocal images are single optical sections. Bundles are counterstained for actin filaments (green). **a**, Labelling (red) of wild-type stereocilia with an antibody against the cytoplasmic domain of murine CDH23 (lateral view of ampullary hair cells in a semicircular canal). **b**, Immunoreactivity is absent in *sputnik*^{t23576} stereocilia. **c**, High magnification view of two wild-type bundles. Note the staining of shorter stereocilia (arrows). **d**, Schematic diagram of the various extracellular links between stereocilia. AL, ankle link; HC, horizontal connector; LL, lateral link; TL, tip link. **e**, Web-like ankle links (arrows) are present near the base of *sputnik*^{tc317e} bundles. **f**, Lateral links or shaft connectors (arrows) are present throughout *sputnik*^{tc317e} bundles. **g**, A horizontal top connector (arrow) in a *sputnik*^{tc317e} hair bundle. **h**, A tip link (arrow) in a wild-type larva. Electron-dense material is present at either end of the tip link (arrowheads). **i**, Absence of a tip link between adjacent stereocilia in a *sputnik*^{tc317e} larva. **j**, **k**, Similar view of stereociliary tips in *sputnik*^{tz300a} (**j**) and *sputnik*^{te370e} (**k**) larvae. Scale bar: 5 μm (**a**, **b**); 2 μm (**c**); 300 nm (**e**); 150 nm (**f**–**k**).

frequently seen in wild-type specimens was never observed in *tc317e* larvae. Other extracellular filaments such as ankle links, lateral links and horizontal top connectors, which are areas of close contact between adjacent stereocilia, appeared unaffected (Fig. 3e–g). In two sections of *tc317e* larvae, we observed a very short link running between stereociliary tips; however, typical electron-dense plaques at either end were absent, suggesting that these were lateral links (Fig. 3i and Supplementary Fig. 3). In contrast to mutant bundles, tip links were readily detectable in wild-type sibling hair bundles (eight bundles of four specimens) in over 85% of all sections examined (Fig. 3h; 1–4 tip links per section, >44 tip links total in 52 sections).

We also examined hair bundles in larvae carrying the weaker *sputnik*^{tz300a} and *sputnik*^{te370e} alleles (75 serial sections of 11 bundles in six *tz300a* larvae; >200 serial sections of 15 bundles in four *te370e* larvae). These alleles cause a complete absence or reduction of extracellular potentials in hair cells, and yet the hair bundles are only slightly splayed. At the electron microscopic level, most of the stereocilia were still organized into bundles in both mutants; however, as with mutant *tc317e* hair bundles, tip links were not detectable (Fig. 3j, k). In four sections of *sputnik*^{te370e} hair bundles some filamentous material at the tips or evidence of tenting was present, suggesting that tip links may occasionally be present (Supplementary Fig. 3). Although the *te370e* mutation does not appear to be a null mutation based on bundle morphology and microphonic potentials, we were unable to detect tip links by serial sectioning. Taken together, our TEM analysis provides strong evidence that Cdh23 is a tip link component, and that tip link defects affect mechanosensory transduction, even in the absence of gross structural defects in hair-cell bundles.

We demonstrate here that Cdh23 localizes to hair bundles, and that tip links are absent in Cdh23-deficient zebrafish. These data strongly suggest that Cdh23 is an essential component of the tip links and presumably kinocilial links, and that it acts as an intracellular adhesion molecule connecting stereocilia to each other and to kinocilia. A recent study has revealed that the tip link appears to be composed of two long filaments that are intertwined[26]. According to this study, the tip link does not appear to be elastic but rather somewhat rigid. It has also been shown that the tip link is sensitive to BAPTA[25]. Both properties would fit a model in which the tip link is composed of cadherin-like molecules that are capable of forming different adhesion complexes of varying lengths and strengths[27,28]. Pairing of different combinations of the 27 ectodomain repeats would impart some flexibility to the tension and length of links.

The weakest allele of *sputnik*, *te370e*, which has an insertion of four amino acids in EC14, is particularly interesting in terms of mechanotransduction. The *sputnik*^{te370e} phenotype is characterized by mainly intact hair bundles and yet extracellular potentials are reduced by two-thirds. Although the addition of four amino acids in EC14 seems to be less detrimental to the integrity of the overall bundle ultrastructure, the insertion critically affects tip links and transduction. At the electron microscopic level, normal tip links appear to be absent in *sputnik*^{te370e} hair bundles, and instead, on rare occasions we found links that were shorter and rather amorphous in comparison with wild-type links. This phenotype suggests that Cdh23 has important functions in mechanosensory transduction that are independent of a structural role in hair cells. Electrophysiological studies have provided evidence that a gating spring regulates the activity of the mechanotransduction channel in hair cells, and the tip link has been proposed to be the gating spring or in series with it[1,25]. Our findings are consistent with this model. The identification of Cdh23 as an essential component of the tip link allows the further study of its function in mechanotransduction, especially with respect to the candidate transduction channel in zebrafish, TRPN1 (also known as NompC)[29]. □

Methods

Zebrafish strains

Six alleles (Tübingen (Tü) background) of *sputnik* (*t23576*, *tc242b*, *tc317e*, *te370e*, *tj264a* and *tz300a*) were used for this study. *alb* larvae in Tü background were used for *in situ* hybridization.

Genetic mapping and positional cloning

Heterozygous fish with the Tü background carrying the mutation *sputnik* (*tj264a*) were crossed to wild-type WIK fish. F_2 mutant larvae were used for meiotic mapping using PCR-able SSLP markers (see mapping scheme at http://www.eb.tuebingen.mpg.de/dept3/geisler/home.html and markers at http://zebrafish.mgh.harvard.edu/cgi-bin/ssr_map). To initiate the chromosomal walk, we used PCR to screen bacterial artificial chromosome (BAC) (BioCat), P1 artificial chromosome (PAC) (Resource Center for the German Genome Project) and yeast artificial chromosome (YAC) (Research Genetics) libraries. PACa corresponds to BUSMP706L06118Q2, PACc to BUSMP706A1551Q0, PACd to BUSMP706H17231Q0 and PACe to BUSMP706B0244Q0.

Sequencing of PACc

The PAC (BUSMP706A1551Q0), with an insert size of 115 kilobases (kb), was sequenced using the shotgun approach[30]. The PAC DNA was sheared, blunt-end-cloned into the pCR4-TOPO vector and transformed into *Escherichia coli* (Shotgun Subcloning Kit, Invitrogen). The plasmid DNA from the shotgun library was prepared using the TurboPrep Kit from Qiagen. Sequencing reactions were performed by use of the BigDye sequencing Kit (Version 2) (AppliedBiosystems) on an ABI prism 3700. The sequencing reads were analysed and assembled as described elsewhere[30].

Sequence analysis

The four *cdh23* exons on PACc were detected by comparing the nucleotide sequence data with other sequences in GenBank using BLAST (http://www.ncbi.nlm.nih.gov/BLAST) and GENSCAN (http://bioweb.pasteur.fr/seqanal/interfaces/genscan-simple.html). The SMART web-based tool (http://smart.embl-heidelberg.de/) was used for protein domain search.

RACE and mutation analyses

The SMART RACE cDNA amplification kit (Clontech) was used for 5′- and 3′-RACE using poly(A)$^+$ RNA from homozygous wild-type larvae (day 5). PCR products were subcloned into the pCRII-TOPO vector (Invitrogen) and sequenced. RNA was prepared from homozygous mutant larvae (day 5) of all five alleles and from homozygous wild-type larvae using the NucleoSpin RNAII Kit (Macherey-Nagel). Reverse transcription reactions were performed by using an oligo(dT) primer and Superscript reverse transcriptase (Invitrogen). Mutations were detected by comparing cDNA of each allele with the wild-type sequence using Lasergene software from DNASTAR. The identified mutations were confirmed at least once with another independent sequence.

Morpholino injections and *in situ* hybridization

Morpholino oligonucleotides were obtained from Gene Tools (Philomath). The ATG morpholino sequence is 5′-CTCCCGAACCTTCACACCACGACAT-3′. The GT morpholino sequence is 5′-TGTTTGAGACACTCACCCACTGGTG-3′. Injections into the yolk were carried out using morpholino concentrations of 0.09–9.0 mg ml^{-1}. For every indicated concentration, $n \geq 30$ larvae were examined. Total RNA was extracted (Nucleospin RNAII, Macherey-Nagel) from pools of ten control or morphant larvae at 3 and 5 d.p.f., then reverse-transcribed using Clontech Moloney murine leukaemia virus and amplified using forward (5′-ACGTGGGTGAAGTTGCTTCTT-3′) and reverse (5′-GAATGGCATAGGGTTGGTTGA-3′) primers amplifying a 403-base-pair (bp) fragment in uninjected larvae and a 325-bp fragment corresponding to the truncated version of the shorter version of the mRNA present in morphant larvae.

Whole-mount *in situ* hybridization was performed as described[31] using a probe from nucleotides 448–1,566.

Phalloidin labelling of hair bundles

Whole larvae (day 5) were fixed as described below and then permeabilized with 2% Triton X-100 overnight at 4 °C. The larvae were then incubated with 2.5 mg ml^{-1} Alexa-fluor-488–phalloidin (Molecular Probes) for >3 h at 4 °C. After rinsing with PBS, the larvae were mounted onto dishes with fine glass fibres and confocal images were made using a ×100 oil lens on a Leica DM IRBE inverted microscope. For all experiments $n \geq 7$ for each allele.

Immunohistochemistry

The primary antibody (CDH23*cyto; see accompanying manuscript[22]) was generated by immunizing rabbits with a fusion protein between glutathione *S*-transferase (GST) and amino acids 3,133–3,291 of murine CDH23 (GenBank number 13399315), which occur within the cytoplasmic domain of CDH23 and include exon 68. The antiserum was affinity purified against the cytoplasmic domain. For whole mounts, larvae (4 d.p.f.) were fixed in 4% paraformaldehyde in PBS and permeabilized by adding 2% Triton X-100 (overnight at 4 °C). After four washing steps with PBST, the larvae were blocked for 1 h at room temperature in PBST with 1% BSA. The primary antibody was used at 1:400 and the incubation was carried out at 4 °C overnight. After washing four times with PBST, the larvae were incubated overnight at 4 °C with the secondary antibody (Alexa-546 goat anti-rabbit IgG antibody; Molecular Probes) and with 2.5 mg ml^{-1} Alexa-fluor-488–phalloidin, then washed four times with PBST.

Electron microscopy

Whole larvae (day 5) were anaesthetized with 0.02% MESAB (3-aminobenzoic acid ethyl ester) and then fixed by immersion in 2.0% glutaraldehyde and 1.0% paraformaldehyde in normal solution (containing (in mM): 145 NaCl, 3 KCl, 1.8 $CaCl_2$, 10 HEPES, pH 7.2) overnight to several days at 4 °C. Specimens were fixed with 1.0% OsO_4 in H_2O for 10 min on ice, followed by fixation and contrast with 1.0% uranyl acetate for 1 h on ice, and then dehydrated with several steps in ethanol and embedded in Epon. Ultrathin sections (90–120 nm) of mutant *sputnik* and wild-type sibling anterior maculae were stained with lead citrate and uranyl acetate. Mutant bundles were serially sectioned at intervals of 1–2 μm or greater; both anterior maculae were present on each section. Wild-type bundles were partially sectioned (0.2–0.6 μm). Cross-sections of bundles contained up to five stereociliary tips (see Supplementary Fig. 2).

Received 12 December 2003; accepted 10 March 2004; doi:10.1038/nature02484.
Published online 31 March 2004.

1. Howard, J. & Hudspeth, A. J. Compliance of the hair bundle associated with gating of mechanoelectrical transduction channels in the bullfrog's saccular hair cell. *Neuron* **3,** 189–199 (1988).
2. Granato, M. *et al.* Genes controlling and mediating locomotion behavior of the zebrafish embryo and larva. *Development* **123,** 399–413 (1996).
3. Nicolson, T. *et al.* Genetic analysis of vertebrate sensory hair cell mechanosensation: the zebrafish circler mutants. *Neuron* **20,** 271–283 (1998).
4. Seiler, C. & Nicolson, T. Defective calmodulin-dependent rapid apical endocytosis in zebrafish sensory hair cell mutants. *J. Neurobiol.* **41,** 424–434 (1999).
5. Bork, J. *et al.* Usher syndrome 1D and nonsyndromic autosomal recessive deafness DFNB12 are caused by allelic mutations of the novel cadherin-like gene CDH23. *Am. J. Genet.* **68,** 26–37 (2000).
6. Bolz, H. *et al.* Mutation of *CDH23*, encoding a new member of the cadherin gene family, causes Usher syndrome type 1D. *Nature Genet.* **27,** 108–112 (2001).
7. Di Palma, F. *et al.* Mutations in *Cdh23*, encoding a new type of cadherin, cause stereocilia disorganization in *waltzer*, the mouse model for Usher syndrome type 1D. *Nature Genet.* **27,** 103–107 (2001).
8. Wilson, S. *et al.* Mutations in Cdh23 cause nonsyndromic hearing loss in waltzer mice. *Genomics* **74,** 228–233 (2001).
9. Wada, T. *et al.* A point mutation in a cadherin gene, Cdh23, causes deafness in a novel mutant, waltzer mouse niigata. *Biochem. Biophys. Res. Comm.* **283,** 113–117 (2001).
10. Siemens, J. *et al.* The Usher syndrome proteins cadherin 23 and harmonin form a complex by means of PDZ-domain interactions. *Proc. Natl Acad. Sci. USA* **99,** 14946–14951 (2002).
11. Boeda, B. *et al.* Myosin VIIa, harmonin and cadherin 23, three Usher I gene products that cooperate to shape the sensory hair cell bundle. *EMBO J.* **21,** 6689–6699 (2002).
12. Pickles, J. *et al.* The organization of tip links and stereocilia on hair cells of bird and lizard basilar papillae. *Hear. Res.* **41,** 31–42 (1989).
13. Goodyear, R. & Richardson, G. Distribution of the 275 kD hair cell antigen and cell surface specializations on auditory and vestibular hair bundles in the chicken inner ear. *J. Comp. Neurol.* **325,** 243–256 (1992).
14. Katori, Y., Tonosaki, A. & Takasaka, T. WGA lectin binding sites of the apical surface of corti epithelium: enhancement by back-scattered electron imaging in guinea-pig inner ear. *J. Elec. Microsc.* **45,** 207–212 (1996).
15. Goodyear, R. & Richardson, G. The ankle-link antigen: an epitope sensitive to calcium chelation associated with the hair-cell surface and the calycal processes of photoreceptors. *J. Neurosci.* **19,** 3761–3772 (1999).
16. Goodyear, R. J. & Richardson, G. P. A novel antigen sensitive to calcium chelation that is associated with the tip links and kinocilial links of sensory hair bundles. *J. Neurosci.* **23,** 4878–4887 (2003).
17. Goodyear, R. J. *et al.* A receptor-like inositol lipid phosphatase is required for the maturation of developing cochlear hair bundles. *J. Neurosci.* **23,** 9208–9219 (2003).
18. Pickles, J. & Corey, D. Mechanoelectrical transduction by hair cells. *Trends Neurosci.* **15,** 254–259 (1992).
19. Steel, K. & Kros, C. A genetic approach to understanding auditory function. *Nature Genet.* **27,** 143–149 (2001).
20. Ernest, S. *et al. Mariner* is defective in *myosin VIIA*: a zebrafish model for human hereditary deafness. *Hum. Mol. Genet.* **9,** 2189–2196 (2000).
21. Riley, B. B., Zhu, C., Janetopoulos, C. & Aufderheide, K. J. A critical period of ear development controlled by distinct populations of ciliated cells in the zebrafish. *Dev. Biol.* **191,** 191–201 (1997).
22. Siemens, J. *et al.* Cadherin 23 is a component of the tip link in hair cell stereocilia. *Nature* advance online publication 31 March 2004 (doi:10.1038/nature02483).
23. Neugebauer, D. & Thurm, U. Surface charges of the membrane and cell adhesion substances determine the structural integrity of hair bundles from the inner ear of fish. *Cell Tissue Res.* **249,** 199–207 (1987).
24. Leckband, D. & Sivasankar, S. Mechanism of homophilic cadherin adhesion. *Curr. Opin. Cell Biol.* **12,** 587–592 (2000).
25. Assad, J., Shepherd, G. & Corey, D. Tip-link integrity and mechanical transduction in vertebrate hair cells. *Neuron* **7,** 987–994 (1991).
26. Kachar, B., Parakkal, M., Kurc, M., Zhao, Y. & Gillespie, P. High-resolution structure of hair cell tip links. *Proc. Natl Acad. Sci. USA* **97,** 13336–13341 (2000).
27. Baumgartner, W. *et al.* Cadherin interaction probed by atomic force microscopy. *Proc. Natl Acad. Sci. USA* **97,** 4005–4010 (2000).
28. Sivasankar, S., Gumbiner, B. & Leckband, D. Direct measurements of multiple adhesive alignments and unbinding trajectories between cadherin extracellular domains. *Biophys. J.* **80,** 1758–1768 (2001).
29. Sidi, S., Friedrich, R. & Nicolson, T. NompC TRP channel required for vertebrate sensory hair cell mechanotransduction. *Science* **301,** 96–99 (2003).
30. Fleischmann, R. D. *et al.* Whole-genome random sequencing and assembly of *Haemophilus influenzae*. *Science* **269,** 496–512 (1995).
31. Westerfield, M. *The Zebrafish Book* 3rd edn (Univ. Oregon Press, Eugene, Oregon, 1995).

Supplementary Information accompanies the paper on **www.nature.com/nature**.

Acknowledgements We thank U. Schönberger, A. Hruscha and members of the electron microscopy laboratory (especially H. Schwarz) at the Max-Planck-Institut für Entwicklungsbiologie for their technical support and advice. This work was supported by funding from the SFB430 and DFG.

Competing interests statement The authors declare that they have no competing financial interests.

Correspondence and requests for materials should be addressed to T.N. (nicolson@ohsu.edu).
The sequence has been deposited in GenBank under accession number AY530192.

The Tübingen 2000 Screen Consortium: **F. van Bebber[1], E. Busch-Nentwich[1], R. Dahm[1], O. Frank[1], H.-G. Frohnhöfer[1], H. Geiger[1], D. Gilmour[1], S. Holley[1], J. Hooge[1], D. Jülich[1], H. Knaut[1], F. Maderspacher[1], H.-M. Maischein[1], C. Neumann[1], C. Nüsslein-Volhard[1], H. Roehl[1], U. Schönberger[1], C. Seiler[1], S. Sidi[1], M. Sonawane[1], A. Wehner[1], P. Erker[2], H. Habeck[2], U. Hagner[2], C. E. Hennen Kaps[2], A. Kirchner[2], T. Koblizek[2], U. Langheinrich[2], C. Loeschke[2], C. Metzger[2], R. Nordin[2], J. Odenthal[2], M. Pezzuti[2], K. Schlombs[2], J. deSantana-Stamm[2], T. Trowe[2], G. Vacun[2], B. Walderich[2], A. Walker[2] & C. Weiler[2]**

Affiliations for authors: 1, Max-Planck-Institut für Entwicklungsbiologie, Spemannstrasse 35, 72076 Tübingen, Germany; 2, Artemis Pharmaceuticals GmbH, 72076 Tübingen, Germany

Splicing of *oskar* RNA in the nucleus is coupled to its cytoplasmic localization

Olivier Hachet & Anne Ephrussi

European Molecular Biology Laboratory, Meyerhofstrasse 1, Postfach 10.2209, D-69117 Heidelberg, Germany

oskar **messenger RNA localization at the posterior pole of the** ***Drosophila*** **oocyte is essential for germline and abdomen formation in the future embryo[1,2]. The nuclear shuttling proteins Y14/Tsunagi and Mago nashi are required for** ***oskar*** **mRNA localization, and they co-localize with** ***oskar*** **mRNA at the posterior pole of the oocyte[3–5]. Their human homologues, Y14/RBM8 and Magoh, are core components of the exon–exon junction complex (EJC)[6–9]. The EJC is deposited on mRNAs in a splicing-dependent manner, 20–24 nucleotides upstream of exon–exon junctions, independently of the RNA sequence[6–8]. This indicates a possible role of splicing in** ***oskar*** **mRNA localization, challenging the established notion that the** ***oskar*** **3′ untranslated region (3′UTR) is sufficient for this process. Here we show that splicing at the first exon–exon junction of** ***oskar*** **RNA is essential for** ***oskar*** **mRNA localization at the posterior pole. We revisit the issue of sufficiency of the** ***oskar*** **3′UTR for posterior localization and show that the localization of unrelated transcripts bearing the** ***oskar*** **3′UTR is mediated by endogenous** ***oskar*** **mRNA. Our results reveal an important new function for splicing: regulation of messenger ribonucleoprotein complex assembly and organization for mRNA cytoplasmic localization.**

To address the requirement of splicing for *oskar* mRNA localization, we tested the effect of deleting *oskar* introns on mRNA localization by a transgenic approach. We evaluated *oskar* mRNA localization in the $osk^{A87}/Df(3R)p^{XT103}$ background, in which no endogenous *oskar* RNA is produced[10]. $osk^{A87}/Df(3R)p^{XT103}$ ovaries